 ©2020 Kvantovaya Elektronika and IOP Publishing Limited

https://doi.org/10.1070/QEL17316

Photoacoustic methane gas analyser based on a 3.3-μm optical parametric oscillator

I.V. Sherstov, D.B. Kolker

Abstract. **We demonstrate a bench-scale prototype of a photoacoustic (PA) methane gas analyser that takes advantage of an optical parametric oscillator (OPO) based on a fan-out MgO : PPLN structure and resonant differential PA detector. The OPO emits in a repetitively pulsed mode (~1750 Hz) at an idler wavelength of ~3.3 μm with an average power of ~40–50 mW. Using the prototype laser PA gas analyser, we experimentally demonstrate the feasibility of measuring the background methane concentration in air (~2–3 ppm of CH_4). The threshold sensitivity of the PA gas analyser (1σ) is determined to be ~ 49 ppb of CH_4.**

Keywords: *methane, photoacoustic gas analyser, optical parametric oscillator, resonant differential photoacoustic detector.*

1. Introduction

In local analysis of the gas composition of the atmosphere and various gas mixtures, wide use is made of instruments that rely on the principles of laser photoacoustic (PA) spectroscopy [1–5] and allow for essentially real-time measurements of analyte gas concentration in a gas sample (in contrast to gas chromatography). The most sensitive PA gas analysers so far have been produced using various types of resonant photoacoustic detectors (PADs) [5–9].

Methane is a greenhouse gas whose emissions can be monitored from satellites [10]. Over the past 200 years, the background CH_4 concentration n_b in air has increased from ~730 ppb (at the beginning of the 19th century) to ~1.86 ppm (in 2019) [11]. In some cases, in studies of the composition of the atmospheric boundary layer under field conditions, real-time measurements of the background methane concentration in air are required. For this purpose, one needs a lightweight, compact, highly sensitive CH_4 gas analyser having an independent power supply and low energy consumption, which can be achieved using laser PA spectroscopy.

A necessary condition for the ability to employ laser PA spectroscopy is that the laser wavelength fall in an absorption band of the gas to be studied. Methane has two strong, broad absorption bands, centred at $\lambda_1 \approx 3.3$ μm and $\lambda_2 \approx 7.7$ μm [12] (Fig. 1a), and a weak absorption band at a wavelength $\lambda_3 \approx$ 1.65 μm (an overtone of the 3.3-μm band, not shown in Fig. 1a), where absorption is about a hundred times weaker than that in the fundamental absorption band of CH_4 at ~3.3 μm. Various research groups use the three above-mentioned absorption bands of CH_4 for monitoring methane: $\lambda_1 \approx 3.3$ μm [13–17], $\lambda_2 \approx 7.7$ μm [18], and $\lambda_3 \approx 1.65$ μm [19–22].

This paper presents a continuation of our previous work concerned with the capabilities of the LaserBreeze laser PA gas analyser [23]. As a light source, this gas analyser uses a combined optical parametric oscillator (OPO) [24] having a continuous wavelength tuning range from 2.5 to 10.8 μm. Karapuzikov et al. [23] presented measured absorption spectra of more than 20 distinct substances.

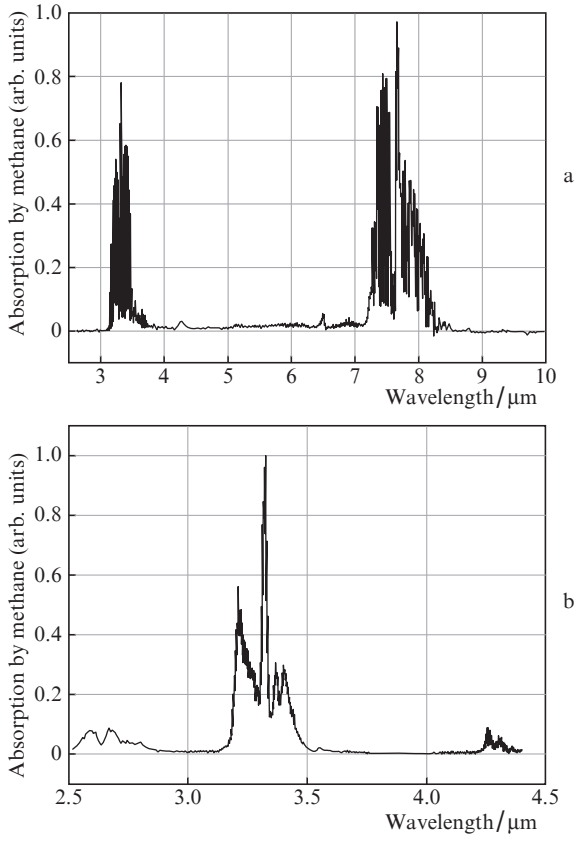

Figure 1. (a) Absorption spectrum of methane in the range 2.5–10 μm from the NIST Standard Reference Database [12] and (b) absorption spectrum of methane (N_2 + 1000 ppm CH_4 gas mixture) measured in the range 2.5–4.5 μm using the PA gas analyser [23] based on a combined OPO with a continuous wavelength tuning range from 2.5 to 10.8 μm.

I.V. Sherstov, D.B. Kolker Institute of Laser Physics, Siberian Branch, Russian Academy of Sciences, prosp. Akad. Lavrent'eva 15b, 630090 Novosibirsk, Russia; Novosibirsk State University, ul. Pirogova 1, 630090 Novosibirsk, Russia; e-mail: sherstov@ngs.ru, dkolker@mail.ru

Received 4 March 2020; revision received 14 May 2020
Kvantovaya Elektronika **50** (11) 1063–1067 (2020)
Translated by O.M. Tsarev

Figure 1b shows the absorption spectrum of methane measured in the range 2.5–4.5 μm using the PA gas analyser in question [23] and a N_2 + 1000 ppm CH_4 gas mixture. The spectral resolution of the PA gas analyser was ~5 cm^{-1}. It is seen that the band centred at ~3.3 μm in the measured absorption spectrum of methane is on the whole similar in shape to that in the absorption spectrum of CH_4 in the NIST Standard Reference Database [12] (Fig. 1a). Note that on the left of Fig. 1b, in the range 2.7–2.8 μm, one can see the absorption spectrum of water vapour, which was present in a small amount in the gas mixture containing methane impurities. In detecting the background CH_4 concentration in air, absorption by water vapour in the atmosphere can be an interference.

The purpose of this work was to experimentally study parameters of a bench PA CH_4 gas analyser based on an ~3.3-μm OPO and a resonant differential PAD.

2. Experimental setup

In our experiments aimed at detecting methane in air, we used an experimental setup schematised in Fig. 2. It comprises a Nd:YLF laser, OPO, resonant differential PAD, pyroelectric detector, air pump, multichannel ADC card, controller, and computer. For simplicity, some of the auxiliary optical components (scanning mirrors, plates, filter, and others) are omitted in the schematic.

The diode-pumped (TECH-1053-N) Nd:YLF laser operates at a wavelength λ_p = 1.053 μm in a repetitively pulsed *Q*-switched mode. The maximum laser pulse energy is ~1.5 mJ, at a pulse duration of ~7 ns. The pulse repetition rate can be varied in the range 10–4000 Hz. Nd:YLF laser pulses are used for optical pumping of a tunable OPO based on a fan-out MgO:PPLN periodically poled structure.

A light beam from the OPO (idler wave, $\lambda_i \approx 3.3$ μm) sequentially passes through a spectral filter (not shown in Fig. 2), a lens, a diaphragm, and the resonant differential PAD and arrives at the pyroelectric detector, which is used to normalise the signal from the differential PAD to the OPO output power. The pulse repetition rate of the OPO is equal to the lowest resonance frequency (f_1) of the differential PAD (~1750–1780 Hz). The electrical signals from the differential PAD (U_1) and pyroelectric detector (U_2) are fed to the inputs of the multichannel ADC card for digitising and then to the computer.

Air was driven through the differential PAD by an air pump. The air flow rate did not exceed 0.6 L min^{-1}. The gas flow through the detector was then laminar, minimising the noise level, which thus did not prevent weak absorption measurements.

All processes in the experimental setup [measurements of the instantaneous resonance frequency f_1 of the differential PAD, control over the pulse repetition rate and idler wavelength of the OPO, acquisition and processing of electrical signals from the differential PAD (U_1) and pyroelectric detector (U_2), information display, and others] were computer-controlled using ILPA application software.

2.1. OPO based on a fan-out MgO:PPLN periodically poled structure

In this study, a fan-out MgO:PPLN periodically poled structure was used for parametric frequency conversion. Its schematic is shown in Fig. 3. The dimensions of the fan-out MgO:PPLN structure used are 50 × 20 × 3 mm (*xyz*), and its period Λ gradually varies along the *y* axis in the range 27.5–32.5 μm. The working faces of the structure have an antireflection coating with a centre wavelength of ~1.5 μm.

The optical cavity of the OPO has a single-pass configuration (in contrast to that reported previously [24]). It is formed by two flat semi-transparent mirrors having multilayer dielectric coatings. The mirrors are placed very close to the end faces of the fan-out MgO:PPLN structure (~0.5-mm gap on each side). The OPO wavelength was tuned by moving the structure across the optical cavity axis (along the *y* axis in Fig. 3) with the help of a stepper motor-driven stage. One motor step led to a displacement of the fan-out MgO:PPLN structure by Δy = 1.25 μm, which corresponded to a frequency change of ~0.12 cm^{-1} per step at a wavelength of 3 μm. An experimentally determined idler wavelength tuning curve for a similar OPO was reported previously [24].

For methane detection, the idler wavelength of the OPO was tuned to $\lambda_i \approx 3.3$ μm (as ascertained from the peak response of the differential PAD when it was filled with a N_2 + 1000 ppm CH_4 gas mixture). The average OPO output power at a pulse repetition rate of ~1750 Hz was ~43 mW. The OPO pulse energy ($\lambda_i \approx 3.3$ μm) at a pulse duration of ~7 ns was then

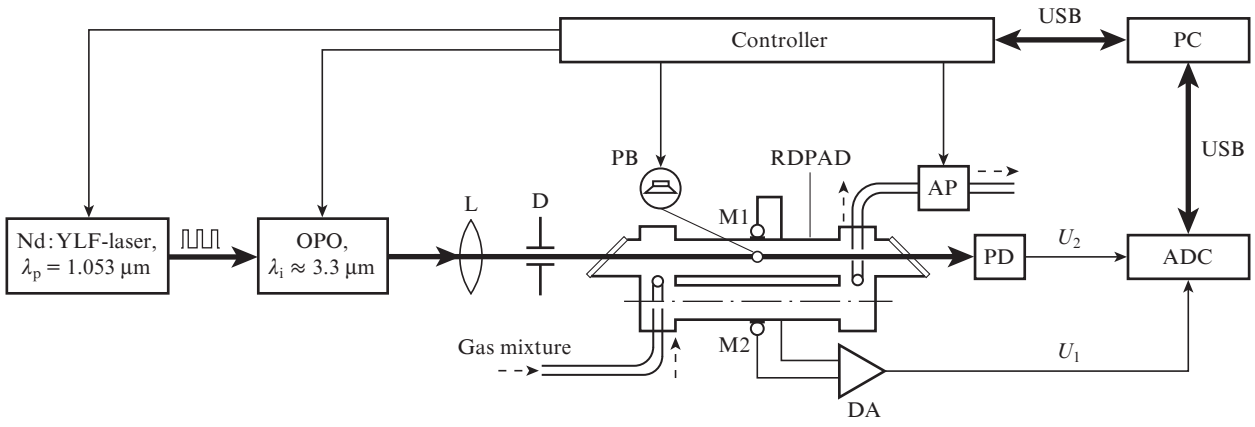

Figure 2. Schematic of the experimental setup:(L) lens (f = 300 mm); (D) diaphragm (∅3 mm); (RDPAD) resonant differential photoacoustic detector; (M1, M2) microphones (EM-6050); (PB) piezoelectric buzzer (CPE-171); (DA) differential amplifier; (PD) pyroelectric detector (MG-30); (AP) air pump; (ADC) analogue-to-digital converter; (PC) computer. The dashed arrows show the air flow direction in the flow regime.

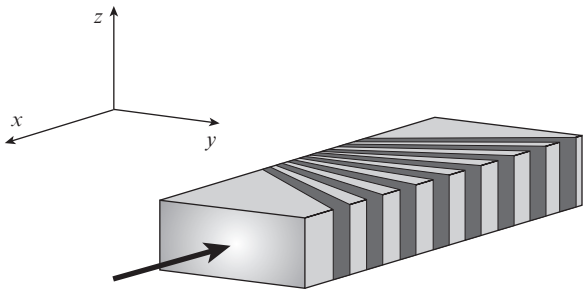

Figure 3. Schematic of the fan-out MgO:PPLN periodically poled structure. The arrow shows the pump beam direction (along the x axis).

~25 μJ, and the light was linearly polarised. The OPO emission bandwidth was ~5 cm^{-1}.

Note that, previously, Sherstov et al. [8] studied parameters of a highly sensitive PA SF_6 gas analyser based on a waveguide CO_2 laser ($\lambda \approx 10.6$ μm) and differential PAD. As shown experimentally [25], an average laser output power of at least 100 mW is necessary and sufficient for reliable detection of ~1 ppb of SF_6 impurities in air. Because of this, the average output power of the OPO in this study approached that recommended in Ref. [25].

2.2. Resonant differential photoacoustic detector

For methane detection, we used a resonant differential photoacoustic detector whose configuration was proposed by Miklos et al. [5].

In our case, the resonant differential PAD (hereafter simply PAD-90) [8, 9] was made of a hard aluminium alloy, had two parallel acoustic resonators (∅9 × 90 mm) separated by a thin wall 1 mm in thickness, and included two buffer cavities (∅20 × 10 mm) closed by flanges with rubber gaskets (Fig. 2). Both flanges had ZnSe windows mounted at Brewster's angle. Gas was introduced into and removed from the PAD-90 through hoses, which were secured on the walls of the buffer cavities.

In the middle of each acoustic resonator of the differential PAD-90, we mounted a microphone (M1, M2), which was connected to a differential amplifier (Fig. 2). To excite acoustic vibrations in the PAD-90 during instantaneous resonance frequency measurements (as described previously [26]), we used a piezoelectric buzzer (PB) located in the centre of one of the acoustic resonators. When the detector was filled with air, its lowest resonance frequency at room temperature was $f_1 \approx$ 1750 Hz (in the case of nitrogen, $f_1^* \approx$ 1780 Hz) [26]. In both cases, the Q-factor of resonances was ~50 (at the –3 dB level).

As shown experimentally, at the lowest resonance frequency f_1 a ring acoustic mode is formed in the differential PAD-90, which was studied previously [27]. A distinctive feature of this ring acoustic mode is that, at the lowest resonance frequency f_1 and in some region around it (about ±500 Hz), antiphase pressure oscillations develop in the two acoustic resonators of the differential PAD-90, whereas at low frequencies (below ~800 Hz) there are in-phase oscillations [27]. Therefore, it is reasonable to connect the two microphones of the PAD-90 to the differential amplifier, which doubles the antiphase (useful) electrical signals from the M1 and M2 microphones and suppresses the in-phase (parasitic) signals. In this case, careful balancing of the two microphones of the differential PAD-90 makes it possible to substantially reduce the low-frequency noise level, including the noise produced by the pump that drives air through the detector.

2.3. Gas impurity concentration measurements

In the optical scheme of the PA gas analyser (Fig. 2), the ratio of the signals (U_1/U_2) measured at the lowest resonance frequency f_1 of the differential PAD-90 can be written in the weak absorption approximation (for the optical thickness of the PA detector $\tau \ll 1$) as

$$\frac{U_1}{U_2} = \frac{1}{T} S_1(f_1) S_2^{-1}(f_1,\lambda) n\sigma(\lambda) l_1, \quad (1)$$

where T is the transmittance of the optical windows of the PAD; $S_1(f_1)$ and $S_2(f_1,\lambda)$ are the sensitivities of the PAD and pyroelectric detector, respectively;

$$n = C(f_1,\lambda)\frac{U_1}{U_2} \quad (2)$$

is the analyte gas concentration in the PAD;

$$C(f_1,\lambda) = \left[\frac{S_2(f_1,\lambda)}{S_1(f_1)}\frac{T}{\sigma(\lambda) l_1}\right]$$

is the calibration factor of the PA methane gas analyser at a wavelength $\lambda_1 \approx 3.3$ μm and the lowest resonance frequency f_1 of the differential PAD; $\sigma(\lambda)$ is the absorption cross section of the analyte gas at wavelength λ; and l_1 is the length of the PAD. In practice, the calibration factor $C(f_1,\lambda)$ of the PA gas analyser is usually determined experimentally via filling of the PAD with a test gas mixture containing a known concentration of the analyte gas.

3. Experimental results

In our experiments, the differential PAD-90 was filled with a test gas mixture containing methane impurities (N_2 + 1000 ppm CH_4), and room air or commercially pure nitrogen was pumped through it. All absorption measurements were performed at atmospheric pressure and room temperature.

Figure 4 shows three 30-s portions of experimental traces of the measured methane concentration calibrated against a N_2 + 1000 ppm CH_4 test gas mixture [see (2)]. Absorption measurements were made at the lowest resonance frequency of the differential PAD-90: f_1 = 1750 Hz (filling with air) or f_1^* = 1780 Hz (filling with nitrogen). The integration time was 0.1 s. The pulse repetition rate of the OPO was equal to the lowest resonance frequency of the differential PAD-90. The output wavelength of the OPO was $\lambda_1 \approx 3.3$ μm, and the average output power was $W \approx 43$ mW.

Region 1 in Fig. 4 is a portion of the experimental trace of the calibrated gas analyser response corresponding to gas concentration n in the PAD-90 filled with a N_2 + 1000 ppm CH_4 test gas mixture (atmospheric pressure, room temperature). Region 2 corresponds to the gas concentration in the PAD-90 while room air is pumped through it (0.6 L min^{-1}), and region 3 corresponds to the gas concentration in the PAD-90 while commercially available nitrogen from a standard high-pressure cylinder is pumped through it at a low flow rate.

It is seen in Fig. 4 that, in the case of the differential PAD-90 filled with the test gas mixture (region 1), the signal from

the PA gas analyser after precalibration corresponds to the methane concentration in the test mixture (n_1 = 1000 ppm of CH_4). In the case of room air flow through the PAD-90 (region 2), the background signal level of the gas analyser corresponds to an equivalent methane concentration $n_2 \approx 3.3$ ppm, which slightly exceeds the typical background CH_4 concentration in air ($n_b \approx 1.86$ ppm [11]). This is attributable to the presence of two to four people in the closed laboratory space (as people exhale a small amount of methane) and the flow of the gas mixture from the cylinder to the room during the experiments. Besides, the high relative humidity of the air and the presence of other hydrocarbon impurities in the air can impair methane detection selectivity as a result of overlap of their absorption spectra.

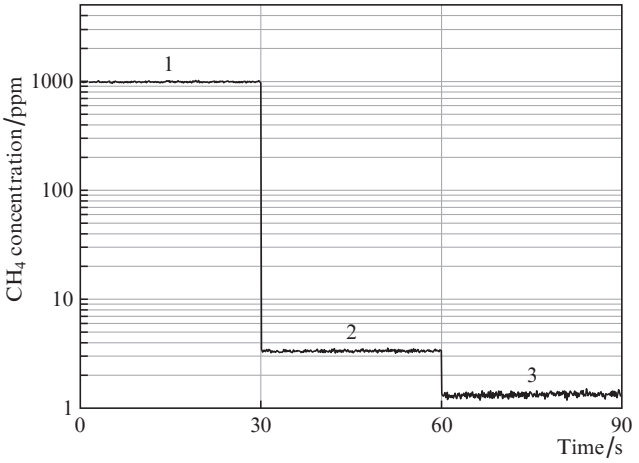

Figure 4. Portions of experimental traces of the methane concentration measured with a bench-scale prototype of the OPO-based PA gas analyser: (1) PAD-90 filled with a N_2 + 1000 ppm CH_4 test gas mixture; (2) pumping of room air through the PAD-90 at a flow rate of 0.6 L min^{-1}; (3) pumping of commercially pure nitrogen from a high-pressure cylinder through the PAD-90 at a low flow rate.

To assess the threshold sensitivity of the PA gas analyser, the differential PAD-90 was filled with commercially pure nitrogen (Fig. 4, region 3) from a standard gas cylinder (at a low gas flow rate in order to preclude the effect of CH_4 desorption from the detector and hose walls). As a result, the background signal level of the PA gas analyser corresponded to an equivalent methane concentration $n_3 \approx 1.3$ ppm, which was about a factor of 1.5 lower than the usual background CH_4 concentration in air ($n_b \approx 1.86$ ppm [11]).

Statistical processing of region 3 of the experimental trace in Fig. 4 (30-s duration, 300 data points) showed that the average equivalent background methane concentration was 1.327 ppm, the standard deviation (1σ) was 0.049 ppm, and the min/max values were 1.198/1.484 ppm. It is seen that the experiment under consideration (methane detection in air) is essentially identical in standard deviation (1σ) to results obtained by Rocha et al. [18] at a wavelength of ~7.7 μm.

Note that, according to its datasheet, the purity of the commercially pure nitrogen in the high-pressure cylinder was 99.6+%. It may be that the use of extrapure nitrogen gas (99.999+% purity) would ensure a considerably lower minimum background signal level of the PA methane gas analyser under consideration.

Thus, it is seen from the present experimental data (Fig. 4) that, at a wavelength of $\lambda_1 \approx 3.3$ μm and laser output power $W \approx 40-50$ mW, methane background concentrations in air at a level of ~2–3 ppm of CH_4 can be detected.

4. Conclusions

We have demonstrated a bench-scale prototype of a photoacoustic methane gas analyser that takes advantage of an OPO based on a fan-out MgO:PPLN structure and resonant differential PA detector. The OPO emits at an idler wavelength of ~3.3 μm with ~40–50 mW of average power. Using the prototype laser PA gas analyser, we have experimentally demonstrated the feasibility of measuring the background methane concentration in air (~2–3 ppm of CH_4). The threshold sensitivity of the PA gas analyser (1σ) was determined to be ~49 ppb of CH_4.

Acknowledgements. We are grateful to N.Yu. Kostyukova, A.A. Boyko, E.Yu. Erushin, L.V. Chetvergova, and V.A. Vasiliev (Institute of Laser Physics, Siberian Branch, Russian Academy of Sciences) for their assistance in the experimental work and with the graphics.

The Nd:YLF laser for optical pumping of the OPO was provided through support from the Russian Science Foundation (Grant No. 19-12-00085).

This work was supported through the National Technology Initiative Programme [Design and Implementation of a Breakthrough Facility for UAV-Based Geophysical Survey Project (Aerotomography)] and the State Research Task No. FSUS-2020-0036.

References

1. Zharov V.P., Letokhov V.S. *Laser Optoacoustic Spectroscopy* (New York: Springer, 1986; Moscow: Nauka, 1984).
2. Ponomarev Yu.N., Ageev B.G., Sigrist M.W., Kapitanov V.A., Courtois D., Nikiforova O.Yu., in *Lazernaya optiko-akusticheskaya spektroskopiya mezhmolekulyarnykh vzaimodeistvii v gazakh* (Optoacoustic Laser Spectroscopy of Intermolecular Interactions in Gases). Ed. by L.N. Sinitsa (Tomsk: MGP RASKO, 2000).
3. Sigrist M., Bartlome R., Marinov D., et al. *Appl. Phys. B*, **90** (2), 289 (2008); https://doi.org/10.1007/s00340-007-2875-4.
4. Harren F.J.M., Cristescu S.M., in *Encyclopedia of Analytical Chemistry* (John Wiley & Sons, Ltd., 2019); https://doi.org/10.1002/ 9780470027318.a0718.pub3.
5. Miklos A., Hess P., Bozoki Z. *Rev. Sci. Instrum.*, **72** (4), 1937 (2001); https://doi.org/10.1063/1.1353198.
6. Harren F.J.M., Bijnen F.G.C., Reuss J., et al. *Appl. Phys. B*, **50** (2), 137 (1990); https://doi.org/10.1007/BF00331909.
7. Fink T., Buscher S., Gabler R., et al. *Rev. Sci. Instrum.*, **67** (11), 4000 (1996); https://doi.org/10.1063/1.1147274.
8. Sherstov I.V., Vasiliev V.A., Zenov K.G., Pustovalova R.V., Spitsyn V.V., Chernikov S.B. *Instrum. Exp. Tech.*, **60** (3), 407 (2017) [*Prib. Tekh. Eksp.*, (3), 106 (2017)]; https://doi.org/10.1134/S0020441217030253.
9. Sherstov I.V., Vasiliev V.A., Karapuzikov A.I., Zenov K.G. *Infrared Phys. Technol.*, **105**, 103170 (2020); https://doi.org/10.1016/j.infrared. 2019.103170.
10. Frankenberg C., Meirink J.F., van Weele M., et al. *Science*, **308** (5724), 1010 (2005); https://doi.org/10.1126/science.1106644.
11. https://www.methanelevels.org (January 25, 2020).
12. NIST Standard Reference Database; https://webbook.nist.gov/chemistry/ (January 25, 2020).
13. Moskalenko K.L., Nadezhdinskii A.I., Stepanov E.V. *Proc. SPIE*, **2205**, 448 (1994); https://doi.org/10.1117/12.166259.
14. Miklos A., Lim C.-H., Hsiang W.-W., et al. *Appl. Opt.*, **41** (15), 2985 (2002); https://doi.org/10.1364/AO.41.002985.

15. Bingi V.N., Stepanov E.V., Chuchalin A.G., Milyaev V.A., Moskalenko K.L., Shulagin Yu.A., Yangurazova L.R. *Tr. Inst. Obshch. Fiz., Ross. Akad. Nauk*, **61**, 189 (2005); https://readera.ru/14343599.
16. Zheng H., Lou M., Tittel F.K., et al. *Opt. Express*, **25** (14), 16761 (2017); https://doi.org/10.1364/OE.25.016761.
17. Lamard L., Balslev-Harder D., Peremans A., et al. *Appl. Opt.*, **58** (2), 250 (2019); https://doi.org/10.1364/AO.58.000250.
18. Rocha M.V., Sthel M.S., Miklos A., et al. *Appl. Phys. B*, **106** (3), 701 (2012); https://doi.org/10.1007/s00340-011-4800-0.
19. Nadezhdinskii A., Berezin A., Chernin S., et al. *Spectrochim. Acta, Part A*, **55** (10), 2083 (1999); https://doi.org/10.1016/S1386-1425(99)00080-3.
20. Kapitanov V.A., Tyryshkin I.S., Ponomarev Yu.N., et al. *Spectrochim. Acta, Part A*, **66** (4-5), 788 (2007); https://doi.org/10.1016/j.saa.2006.10.036.
21. Kapitanov V.A., Ponomarev Yu.N., Tyryshkin I.S., Rostov A.P. *Spectrochim. Acta, Part A*, **66** (4-5), 811 (2007); https://doi.org/10.1016/j.saa.2006.10.046.
22. Wang J., Wang H., Liu X. *Sensors*, **16** (9), 1551 (2016); https://doi.org/10.3390/s16091551.
23. Karapuzikov A.A., Sherstov I.V., Kolker D.B., et al. *Phys. Wave Phenom.*, **22** (3), 189 (2014); https://doi.org/10.3103/S1541308 X14030054.
24. Kolker D.B., Sherstov I.V., Kostyukova N.Yu., Boyko A.A., Zenov K.G., Pustovalova R.V. *Quantum Electron.*, **47** (1), 14 (2017) [*Kvantovaya Elektron.*, **47** (1), 14 (2017)]; https://doi.org/10.1070/QEL16238.
25. Sherstov I.V., Vasiliev V.A., Karapuzikov A.I., Zenov K.G., Pustovalova R.V. *Instrum. Exp. Tech.*, **61** (4), 583 (2018) [*Prib. Tekh. Eksp.*, (4), 117 (2018)]; https://doi.org/10.1134/S0020441218030259.
26. Sherstov I.V., Vasiliev V.A., Goncharenko A.M., Zenov K.G., Pustovalova R.V., Karapuzikov A.I. *Instrum. Exp. Tech.*, **59** (5), 749 (2016) [*Prib. Tekh. Eksp.*, (5), 133 (2016)]; https://doi.org/10.1134/S0020441216050079.
27. Sherstov I., Chetvergova L. *Opt. Commun.*, **462**, 125184 (2020); https://doi.org/10.1016/j.optcom.2019.125184.